

STEADY-STATE PENETRATION OF TRANSVERSELY ISOTROPIC RIGID/PERFECTLY PLASTIC TARGETS

R. C. BATRA† and A. ADAM

Department of Mechanical and Aerospace Engineering and Engineering Mechanics,
University of Missouri-Rolla, Rolla, MO 65401-0249, U.S.A.

(Received 11 December 1990)

Abstract—Axisymmetric deformations of a transversely isotropic, rigid/perfectly plastic target being penetrated by a long rigid cylindrical rod with an ellipsoidal nose have been analyzed. The deformations of the target appear steady to an observer situated at the penetrator nose tip. The contact between the target and the penetrator is assumed to be smooth. Computed results show that the deformation field adjacent to the penetrator nose surface is significantly influenced by the nose shape, and the ratio of the yield stress in the axial direction to that in the transverse direction. The axial resisting force experienced by the penetrator is found to depend strongly upon the nose shape and the ratio of the yield stress in the axial to that in the transverse direction, but weakly upon the square of the penetration speed.

1. INTRODUCTION

For very thick targets, the steady-state portion of the penetration process constitutes a significant part of the entire penetration event. Accordingly, a considerable amount of work has been done in studying this process. For example, Tate [1, 2] and Alekseevskii [3] have modified models in which the steady deformations of the target and the penetrator are assumed to be governed by purely hydrodynamic incompressible flow processes by incorporating the effects of the material strengths of the target and the penetrator. These strengths were assumed to be some multiple of the yield stress of the respective materials, the multiplying factor has recently been given by Tate [4, 5] by using a solenoidal fluid flow model. Pidsley [6], Batra and Gobinath [7], and Batra and Chen [8] have estimated these multiplying factors from their numerical solutions of the problem.

We refer the reader to the review articles of Backmann and Goldsmith [9], Wright and Frank [10], Anderson and Bodner [11], and books by Zukas *et al.* [12], Blazynski [13], and Macauley [14] for a discussion of various aspects of the penetration problem, and for a list of references on the subject. Ravid and Bodner [15], Ravid *et al.* [16], Forrestal *et al.* [17], and Batra and Chen [8] have proposed engineering models of different complexity.

The works referred to above have assumed the target material to be isotropic. However, manufacturing processes such as rolling induce anisotropy in the material properties. For example, in heavily-rolled brass, the tensile yield stress transverse to the direction of rolling may be as much as ten percent greater than that parallel to the direction of rolling [18]. Greater variations may be obtained by an appropriate combination of mechanical and heat treatments,

which produces a final recrystallization texture close to that of a single crystal [19]. Here we assume the target material to be transversely isotropic, and study the effect of varying the yield stress in the axial direction upon the deformation fields during steady-state penetration of the target by a rigid cylindrical penetrator. It is assumed that the degree of anisotropy, defined as the ratio of the yield stress in the axial direction to that in the transverse direction, stays constant during the deformation process. The effect of the speed of penetration as well as the nose shape on the deformations of the target is also investigated.

2. FORMULATION OF THE PROBLEM

We use a cylindrical coordinate system with origin at the center of the penetrator nose and z -axis pointing into the target. We presume that the deformations of the target are axisymmetric and appear steady to an observer situated at the penetrator nose tip and moving with it at a uniform velocity $v_0 \mathbf{e}$, \mathbf{e} being a unit vector in the direction of motion of the rigid penetrator, which we take to be the z -axis. Equations governing the target deformations are

$$\text{div } \mathbf{v} = 0, \quad (2.1)$$

$$\rho(\mathbf{v} \cdot \text{grad})\mathbf{v} = \text{div } \boldsymbol{\sigma}. \quad (2.2)$$

Here \mathbf{v} is the velocity of a target particle relative to the observer situated at the penetrator nose tip, ρ is the mass density for the target material, and $\boldsymbol{\sigma}$ is the Cauchy stress tensor. We neglect elastic deformations of the target and have assumed in (2.1) that its deformations are isochoric. Equations (2.1) and (2.2) express, respectively, the balance of mass and the balance of linear momentum.

We assume that the target material obeys Hill's yield criterion [20], which for transversely isotropic

†Also Senior Research Investigator, Intelligent Systems Center.

materials undergoing axisymmetric deformations becomes

$$F[(\sigma_{yy} - \sigma_{zz})^2 + (\sigma_{zz} - \sigma_{xx})^2] + H(\sigma_{xx} - \sigma_{yy})^2 + 2M\sigma_{xz}^2 = 1, \quad (2.3)$$

where

$$\begin{aligned} 2F &= 1/\bar{\sigma}_{xx}^2, \\ 2H &= 2/\bar{\sigma}_{xx}^2 - 1/\bar{\sigma}_{zz}^2, \\ 2M &= 1/\bar{\sigma}_{xz}^2, \end{aligned} \quad (2.4)$$

$\bar{\sigma}_{xx}$ and $\bar{\sigma}_{zz}$ are yield stresses in the x - and z -directions, respectively, and $\bar{\sigma}_{xz}$ is the shear yield stress.

The constitutive relation for the target material can be written as

$$\boldsymbol{\sigma} = -p\mathbf{1} + \mathbf{s}, \quad (2.5)$$

$$\begin{Bmatrix} s_{rr} \\ s_{\theta\theta} \\ s_{zz} \end{Bmatrix} = \frac{1}{EI} \begin{bmatrix} 3F + H & H & F \\ H & 3F + H & F \\ F & F & 2(F + H) \end{bmatrix} \begin{Bmatrix} D_{rr} \\ D_{\theta\theta} \\ D_{zz} \end{Bmatrix}, \quad (2.6)$$

$$s_{rz} = D_{rz}/MI, \quad (2.7)$$

$$E = 3F(F + 2H), \quad (2.8)$$

$$I^2 = \frac{F(D_{rr}^2 + D_{\theta\theta}^2) + HD_{zz}^2}{F(F + 2H)} + \frac{2}{M} D_{rz}^2, \quad (2.9)$$

$$2\mathbf{D} = \text{grad } \mathbf{v} + (\text{grad } \mathbf{v})^T. \quad (2.10)$$

In eqn (2.5), $\boldsymbol{\sigma}$ is the Cauchy stress tensor, \mathbf{s} the deviatoric stress tensor, and p the hydrostatic pressure not determined by the deformation history. Equations (2.6) and (2.7) relate the components of the deviatoric stress tensor to the components of the strain-rate tensor \mathbf{D} . Note that because of the dependence of I upon D_{rr} , $D_{\theta\theta}$, D_{zz} , and D_{rz} , even s_{rz} depends upon all non-zero components of \mathbf{D} . Equations (2.6)–(2.9) reduce to those for isotropic rigid/perfectly plastic materials if one takes $F = H = 0.5/\sigma_0^2$, $M = 1.5/\sigma_0^2$, σ_0 being the yield stress in a quasistatic simple tension or compression test.

Equation (2.1) and the one obtained by substituting from eqns (2.6)–(2.10) into eqn (2.2) are the field equations to be solved for p and \mathbf{v} subject to suitable boundary conditions. Before stating these, we non-dimensionalize the variables as follows:

$$\begin{aligned} \hat{\sigma} &= \boldsymbol{\sigma}/\sigma_0, & \hat{\mathbf{v}} &= \mathbf{v}/v_0, \\ \hat{r} &= r/r_0, & \hat{z} &= z/r_0, \\ \hat{p} &= p/\sigma_0, & \hat{\mathbf{s}} &= \mathbf{s}/\sigma_0. \end{aligned} \quad (2.11)$$

Here r_0 is the radius of the cylindrical portion of the

penetrator and σ_0 is a reference stress. Rewriting eqns (2.1) and (2.2) in terms of non-dimensional variables, dropping the superimposed hats, and denoting the gradient and divergence operators in non-dimensional coordinates by grad and div , we obtain the following equations

$$\text{div } \mathbf{v} = 0, \quad (2.12)$$

$$\alpha(\mathbf{v} \cdot \text{grad})\mathbf{v} = -\text{grad } p + \text{div } \mathbf{s}, \quad (2.13)$$

where $\alpha = \rho v_0^2/\sigma_0$ is a non-dimensional number and measures the magnitude of inertia forces relative to the flow stress of the material. At the target/penetrator interface we impose

$$\mathbf{t} \cdot (\boldsymbol{\sigma} \mathbf{n}) = 0, \quad (2.14)$$

$$\mathbf{v} \cdot \mathbf{n} = 0, \quad (2.15)$$

where \mathbf{n} and \mathbf{t} are, respectively, the unit outward normal and the unit tangent vectors at a point on the surface. At points far away from the penetrator

$$|\mathbf{v} + \mathbf{e}| \rightarrow 0 \quad \text{as } (r^2 + z^2)^{1/2} \rightarrow \infty, \quad z > -\infty, \quad (2.16)$$

$$|\boldsymbol{\sigma} \mathbf{n}| \rightarrow 0 \quad \text{as } z \rightarrow -\infty. \quad (2.17)$$

The boundary condition (2.14) states that the target/penetrator interface is smooth, and (2.15) implies that there is no penetration of the target material into the penetrator. Equation (2.16) implies that target particles at a large distance from the penetrator appear to be moving at a uniform speed with respect to it, and eqn (2.17) states that far to the rear the traction field vanishes. Note that the governing eqns (2.13) with \mathbf{s} given by (2.6) and (2.7) are nonlinear in \mathbf{v} , and that a solution of the boundary-value problem stated above, if there exists one, will depend on the rate at which quantities in (2.16) and (2.17) tend to zero. Since the problem is difficult to solve analytically, we seek an approximate solution of the problem by the finite element method.

3. FINITE ELEMENT SOLUTION OF THE PROBLEM

3.1. Computational considerations

Recalling that the target deformations are assumed to be axisymmetric, only the finite region R shown in Fig. 1 is studied, and the boundary conditions (2.16) and (2.17) are replaced by the following

$$\begin{aligned} v_z &= -1.0, & v_r &= 0, \\ & & & \text{on the boundary surface EFA,} \end{aligned} \quad (3.1)$$

$$\begin{aligned} \sigma_{zz} &= 1, & v_r &= 0, \\ & & & \text{on the bottom surface AB.} \end{aligned} \quad (3.2)$$

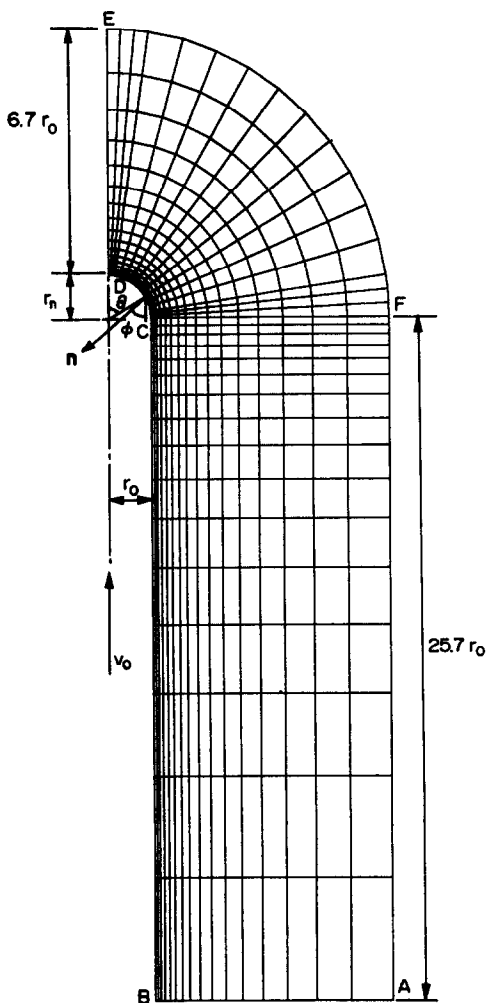


Fig. 1. The finite region analyzed and its discretization.

On the axis of symmetry DE, we impose

$$\sigma_{rz} = 0, \quad v_r = 0. \tag{3.3}$$

A finite element solution of the problem defined by eqns (2.12) and (2.13) with s given by non-dimensionalized versions of (2.6)–(2.10), and boundary conditions (2.14), (2.15), and (3.1)–(3.3) has been found for several values of α , $\bar{\sigma}_{zz}/\bar{\sigma}_{xx}$, and penetrator nose shapes. The finite element code developed by Batra [21] was modified to solve the present problem. The changes made were checked by solving the same penetration problem for an isotropic target with the modified code by setting $F = H = 0.5$, and $M = 1.5$, and with the original code. Since in the numerical solution of the problem, eqn (2.12) is only approximately satisfied, the two sets of results for the same problem computed with the original code and the modified code, as shown in Fig. 2, agree qualitatively, but differ quantitatively by about ten percent. We have used the method of Lagrange multipliers to satisfy the incompressibility constraint (2.12), and the boundary condition (2.15).

3.2. Results for the transversely isotropic target

We have assigned the following values to various variables when computing numerical results that are presented below

$$\begin{aligned} \sigma_0 = \bar{\sigma}_{xx} = \bar{\sigma}_{yy} &= 498 \text{ MPa,} \\ \rho &= 7860 \text{ kg/m}^3, \quad r_0 = 2.54 \text{ mm.} \end{aligned} \tag{3.4}$$

The effect of varying $\bar{\sigma}_{zz}$, v_0 , and the penetrator nose shape is analyzed. The value of $\bar{\sigma}_{xx}$ is computed from

$$\frac{1}{\bar{\sigma}_{xx}^2} = \frac{1}{\bar{\sigma}_{xx}^2} + \frac{2}{\bar{\sigma}_{zz}^2}. \tag{3.5}$$

Except when discussing the effect of the nose shape

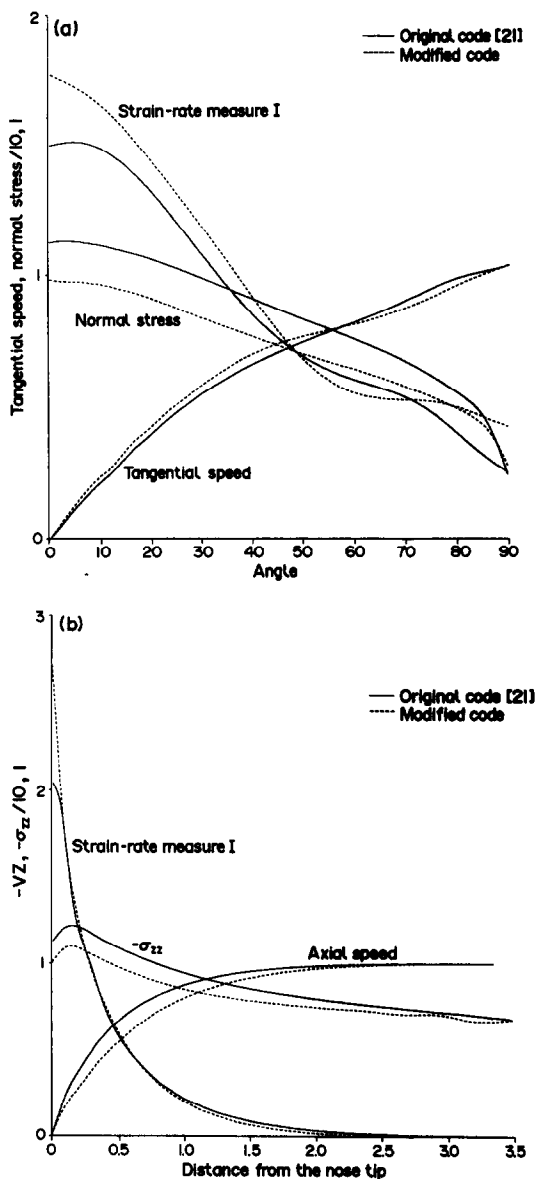


Fig. 2. Comparison of results for an isotropic target computed with the two codes.

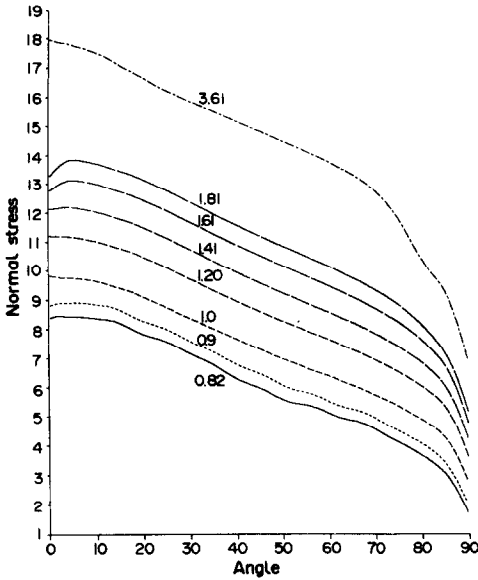


Fig. 3. Effect of the yield stress in the axial direction on the distribution of the normal stress at target particles on the penetrator nose surface. $\alpha = 6.25$.

on the deformations of the target, the penetrator nose is taken to be hemispherical.

Figure 3 shows the effect of the yield stress in the axial direction on the distribution of the normal stress at target particles situated on the penetrator/target interface when $\alpha = 6.25$. As expected, the magnitude of the normal stress increases with an increase in the value of $\bar{\sigma}_{zz}$. The range of values of $\bar{\sigma}_{zz}$ considered is considerably more than that likely to occur in a practical situation. In Figure 4, we have plotted the variation with $\bar{\sigma}_{zz}$ of the strain-rate measure I and the tangential speed at target particles abutting the

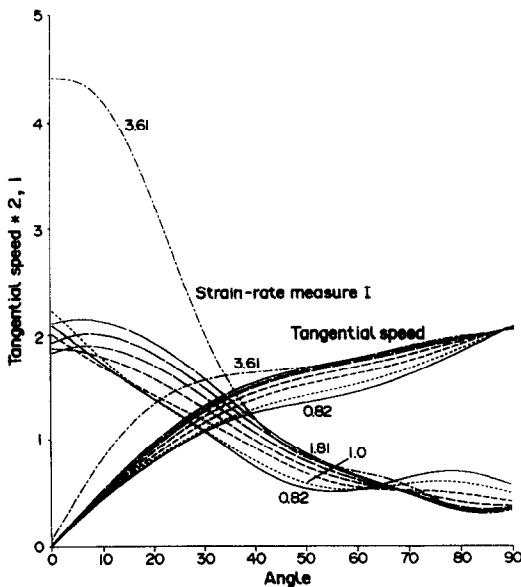


Fig. 4. Effect of the yield stress in the axial direction on the strain-rate measure I and the tangential speed at target particles on the penetrator nose surface. $\alpha = 6.25$.

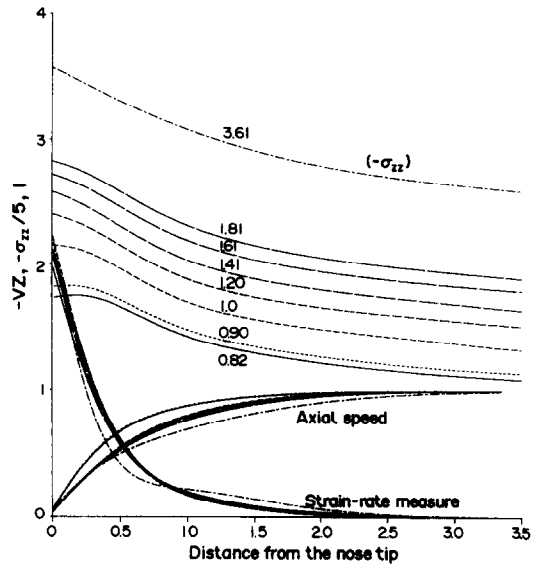


Fig. 5. Effect of the yield stress in the axial direction on I , σ_{zz} , and v_z at target particles on the axial line. $\alpha = 6.25$.

penetrator nose surface for a hemispherical nosed penetrator and $\alpha = 6.25$. At every target particle on the penetrator nose surface, both the tangential speed and the strain-rate measure I increase with $\bar{\sigma}_{zz}$. The tangential speed varies slowly with the value of $\bar{\sigma}_{zz}$ at a target particle on the penetrator nose periphery. The dependence of $(-\sigma_{zz})$, I , and the axial velocity at target particles on the axial line upon the yield stress $\bar{\sigma}_{zz}$ is depicted in Fig. 5. The rate of decay of the axial velocity as seen by an observer moving with the penetrator nose tip decreases with an increase in the value of $\bar{\sigma}_{zz}$. We note that the values of I and the absolute axial velocity become zero at target particles on the axial line whose distance from the penetrator nose tip exceeds $3r_0$. Thus, the region studied is adequate. The values of σ_{zz} do not decay to zero, but approach the value of p as we move away from the penetrator nose surface. We recall that we have neglected elastic deformations of the target, and the hydrostatic pressure does not influence the yielding of the material. The consideration of elastic deformations should give a better estimate of the hydrostatic pressure at a point.

The distributions of the normal stress and the strain-rate measure I at target particles adjoining the target/penetrator interface for four different nose shapes, i.e. $r_n/r_0 = 0.2, 0.5, 1.0, \text{ and } 2.0$, are shown in Fig. 6. Here $2r_0$ and $2r_n$ equal the length of the principal axes in the r and z directions, respectively, of the penetrator nose. The normal stress at the stagnation point appears to be the same for all four different nose shapes. The normal stress decreases rapidly with the angular position θ for a long narrow nose. For the essentially blunt nose, the normal stress stays virtually constant on the entire nose surface, and rapidly drops to zero near the nose periphery. A similar behavior was found by Batra for an isotropic

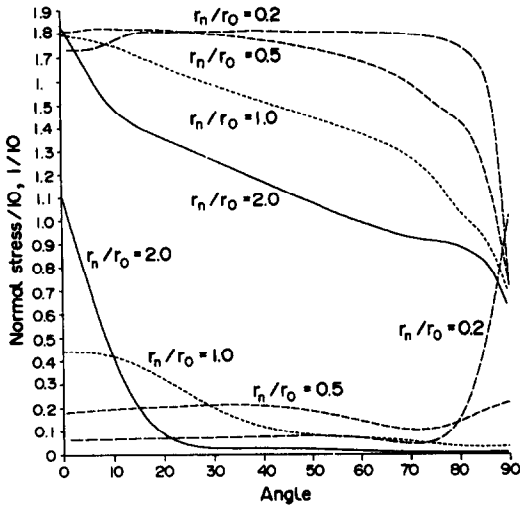


Fig. 6. Distribution of the normal stress and the strain-rate measure I at target particles on the penetrator nose surface for four different shapes of the penetrator nose.

viscoplastic [21] and an isotropic thermoviscoplastic target [22]. For a cylindrical penetrator with a long pointed nose, the strain-rate measure I assumes highest values at the stagnation point, and the values of I drop off sharply with the angular position θ . However, for a blunt nose, I stays essentially constant at a relatively low value on the entire surface and suddenly shoots up near the nose periphery. Thus, very severe deformations of the target occur at points surrounding the stagnation point for a long tapered nosed penetrator, and near the nose periphery for a blunt nosed penetrator. The variation of I , $(-v_z)$, and $(-\sigma_{zz})$ at target particles on the axial line for four different nose shapes is depicted in Fig. 7. The value of the axial velocity changes rather slowly for a blunt

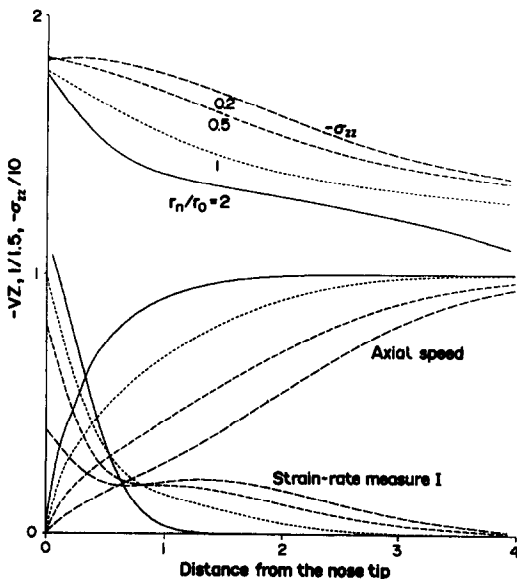


Fig. 7. Distribution of I , v_z , and σ_{zz} at target particles on the axial line for four different shapes of the penetrator nose.

nosed penetrator, but quite rapidly for a long tapered nosed penetrator. The difference in the values of $(-\sigma_{zz})$ at a point on the axial line distant $4r_0$ from the penetrator nose tip is mainly due to the different limiting values of the hydrostatic pressure for the four nose shapes. Ideally, the pressure should decay to zero at target points far away from the penetrator nose. However, the assumption that the target material is rigid/perfectly plastic and the observation that the strain-rates are extremely small at target points whose distance from the penetrator nose tip exceeds $4r_0$ suggest that the computed values of p at target particles far away from the penetrator nose surface are not very reliable.

In Fig. 8, we have plotted for a hemispherical nosed penetrator and $\bar{\sigma}_{zz}/\sigma_0 = 1.8$ the distribution of the normal stress, I , and the tangential speed for different values of α . As for an isotropic target [21], the normal stress at target particles near the nose periphery decreases with α . The tangential speed and the values of I seem to be affected very little by the value of α . At target particles situated on the axial line, the values of σ_{zz} , I , and v_z do not change much when α is increased from 3.0 to 6.25. Their plots and those for $\bar{\sigma}_{zz}/\sigma_0 = 3.6$ are not included in the paper. We note that results for $\bar{\sigma}_{zz}/\sigma_0 = 3.6$ are qualitatively similar to those for $\bar{\sigma}_{zz}/\sigma_0 = 1.8$.

Figure 9 shows the variation of the axial speed v_z with r on the planes $z = 0$ and $z = -1.0$ for the four different nose shapes. These results indicate that the target material adjacent to the sides of the penetrator appears to extrude rearward as a uniform block that is separated from the bulk of the stationary target material by a narrow region with a sharp velocity gradient. This observation provides a partial justification for the velocity field assumed by Ravid and

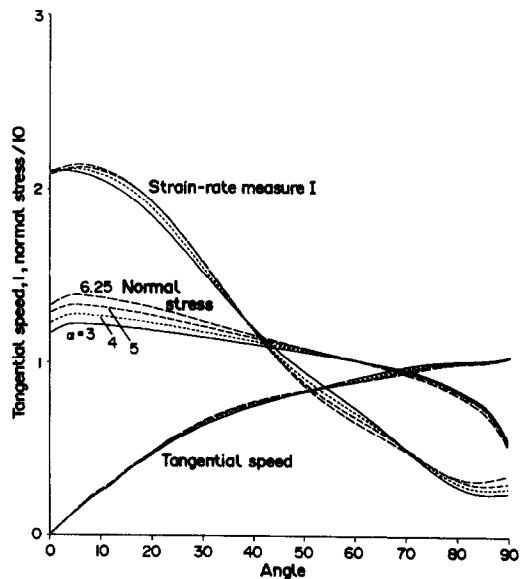


Fig. 8. Distribution of the normal stress, I , and the tangential speed on the penetrator nose surface for different values of α .

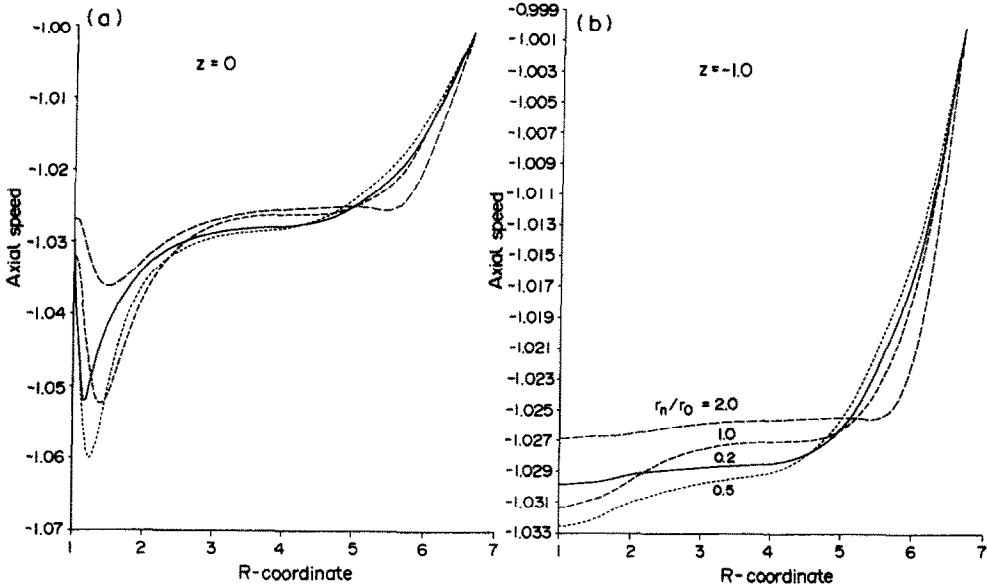


Fig. 9. Variation of the axial speed with r on the surfaces $z = 0$ and $z = -1.0$.

Bodner [15] in their work involving targets of finite thickness. We add that Batra and Wright [23] found a similar result for the steady state penetration of isotropic rigid/perfectly plastic targets.

The axial resisting force F experienced by the penetrator is given by

$$F = 2 \int_0^{\pi/2} (\mathbf{n} \cdot \boldsymbol{\sigma} \mathbf{n}) \times \frac{\cos \phi \sin \theta [\sin^2 \theta + (r_0/r_n)^4 \cos^2 \theta]^{1/2}}{[\sin^2 \theta + (r_0/r_n)^2 \cos^2 \theta]^2} d\theta, \quad (3.6)$$

$$\cos \phi = \frac{z/r_n^2}{[(r/r_0)^2 + (z/r_n^2)^2]^{1/2}}, \quad (3.7)$$

where the angle θ is defined in Fig. 1, and (r, z) are the coordinates of a point on the penetrator/target interface. The corresponding axial force in physical units is given by $(\pi r_0^2 \sigma_0)F$. We note that the expression given by Batra [21] for the axial force, except for the hemispherical nose shape, is in error. The dependence of the axial force upon α , r_n/r_0 , and $\bar{\sigma}_{zz}/\sigma_0$ is exhibited in Fig. 10. For each one of the two values of $\bar{\sigma}_{zz}/\sigma_0$ considered herein, F depends upon α very weakly. However, F depends strongly upon r_n/r_0 and $\bar{\sigma}_{zz}/\sigma_0$; the resisting force is maximum for a blunt nosed and least for a tapered nosed penetrator. F increases rapidly with $\bar{\sigma}_{zz}$ first, but slowly after $\bar{\sigma}_{zz}/\sigma_0$ exceeds approximately 1.9.

4. CONCLUSIONS

We have studied the steady state penetration of a rigid/perfectly plastic and transversely isotropic target being penetrated by a rigid cylindrical penetrator having an ellipsoidal nose. It is found that the

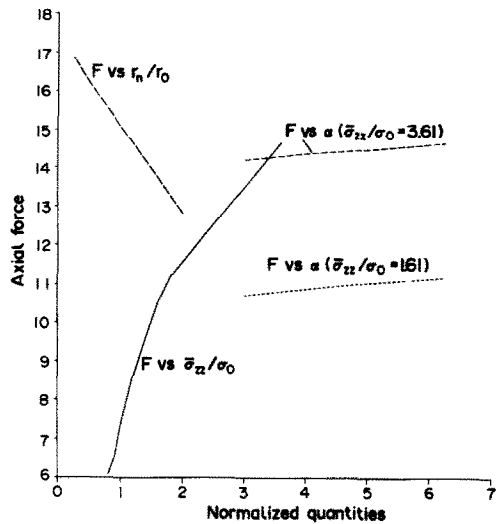


Fig. 10. Dependence of the axial resisting force upon various parameters.

axial resisting force experienced by the penetrator depends strongly upon the penetrator nose shape, and also upon the ratio of the yield stress in the axial direction to that in a transverse direction. The axial resisting force depends rather weakly upon the square of the penetration speed. Peak values of the strain-rate measure I occur near the stagnation point for a long tapered nosed penetrator, but near the nose periphery for a blunt nosed penetrator.

Acknowledgements—This work was supported by the U.S. Army Research Office Contract DAAL03-89-K-0050 to the University of Missouri-Rolla. Some of the computations were performed on the NSF Supercomputer Center in Urbana, Illinois.

REFERENCES

1. A. Tate, A theory for the deceleration of long rods after impact. *J. Mech. Phys. Solids* **15**, 387–399 (1967).
2. A. Tate, Further results in the theory of long rod penetration. *J. Mech. Phys. Solids* **17**, 141–150 (1969).
3. V. P. Alekseevskii, Penetration of a rod into a target at high velocity. *Comb. Expl. and Shock Waves* **2**, 63–66 (1966). (Translation from Russian, Faraday Press, New York.)
4. A. Tate, Long rod penetration models—part II. Extensions to the hydrodynamic theory of penetration. *Int. J. Mech. Sci.* **28**, 599–612 (1986).
5. A. Tate, A simple hydrodynamic model for the strain field in a target by the penetration of a high speed long rod projectile. *Int. J. Engng Sci.* **16**, 858 (1978).
6. P. H. Pidsley, A numerical study of long rod impact onto a large target. *J. Mech. Phys. Solids* **32**, 315–333 (1984).
7. R. C. Batra and T. Gobinath, Steady state axisymmetric deformations of a thermoviscoplastic rod penetrating a thick thermoviscoplastic target. *Int. J. Impact Engng* **11**, 1–31 (1991).
8. R. C. Batra and Xingju Chen, An approximate analysis of steady state axisymmetric deformations of viscoplastic targets. *Int. J. Engng. Sci.* **29**, 1347–1358 (1990).
9. M. E. Backmann and W. Goldsmith, The mechanics of penetration of projectiles into targets. *Int. J. Engng Sci.* **16**, 1–99 (1978).
10. T. W. Wright and K. Frank, *Approaches to Penetration Problems*. SMIRT Symposium, No. 14, Impact, Lausanne, Switzerland (1987).
11. C. E. Anderson and S. R. Bodner, The status of ballistic impact modeling. *Int. J. Impact Engng* **7**, 9–35 (1988).
12. J. A. Zukas *et al.*, *Impact Dynamics*. Wiley-Interscience, New York (1982).
13. T. Z. Blazynski, in *Materials at High Strain Rates*, (Edited by T. Z. Blazynski). Elsevier Applied Science, London (1987).
14. M. Macauley, *Introduction to Impact Engineering*. Chapman & Hall, London (1987).
15. M. Ravid and S. R. Bodner, Dynamic perforation of viscoplastic plates by rigid projectiles. *Int. J. Engng Sci.* **21**, 577–591 (1983).
16. M. Ravid S. R. Bodner and I. Holcman, Analysis of very high speed impact. *Int. J. Engng Sci.* **25**, 473–482 (1987).
17. M. J. Forrestal, K. Okajima and V. K. Luk, Penetration of 6061-T651 aluminum targets with rigid long rods. *J. Appl. Mech.* **55**, 755–760 (1988).
18. M. Cook, *J. Inst. Metals* **60**, 159 (1937).
19. W. M. Baldwin, Jr, *Trans. Am. Inst. Min. Met. Engng* **166**, 591 (1946).
20. R. Hill, *The Mathematical Theory of Plasticity*. Oxford University Press (1960).
21. R. C. Batra, Steady state penetration of viscoplastic targets. *Int. J. Engng Sci.* **25**, 1131–1141 (1987).
22. R. C. Batra, Steady state penetration of thermoviscoplastic targets. *Comp. Mech.* **3**, 1–12 (1988).
23. R. C. Batra and T. W. Wright, Steady state penetration of rigid perfectly plastic targets. *Int. J. Engng Sci.* **24**, 41–54 (1986).